Science

AAAS

Probing the Accumulation History of the Voluminous Toba Magma
Jorge A. Vazquez, *et al.*
Science **305**, 991 (2004);
DOI: 10.1126/science.1096994

Table 1. Least-squares fits to the acceleration data for two masses on Ganymede's surface and also for three masses on the surface. The three independent variables in the fitting model for each mass are Gm, and the geographic coordinates latitude and west longitude. For reference, the closest approach location is at latitude 79.3° and west longitude 123.7° at an altitude of 264 km. The measure of goodness of fit is given by the variance σ^2 for the acceleration residuals. A qualitative measure of the goodness of fit is given by Fig. 3.

	First mass	Second mass	Third mass
Six-parameter fit for two masses ($\sigma^2 = 0.0244$ mgal^2)			
Gm (km^3 s^{-2})	0.0237 ± 0.0056	-0.0558 ± 0.0084	–
Latitude (°)	58.9 ± 1.5	24.2 ± 5.5	–
Longitude W (°)	65.2 ± 1.6	61.8 ± 5.4	–
Nine-parameter fit for three masses ($\sigma^2 = 0.0192$ mgal^2)			
	First mass	Second mass	Third mass
Gm (km^3 s^{-2})	0.0256 ± 0.0038	-0.0500 ± 0.0058	0.0081 ± 0.0021
Latitude (°)	77.7 ± 1.0	39.9 ± 2.6	53.6 ± 2.3
Longitude W (°)	337.3 ± 5.1	355.6 ± 4.6	140.1 ± 4.8

(E12) at an altitude of 201 km. The E12 closest approach point is near the equator at a latitude of −8.7° and a west longitude of 225.7°. However, unlike G2 at an altitude of 264 km, Doppler data from E12, as well as three other more distant flybys (E4 at 692 km, E6 at 586 km, and E11 at 2043 km), can be fit to the noise level with second-degree harmonics. The two Callisto flybys that yield gravity information are more distant (C10 at 535 km and C21 at 1048 km). No anomalies are required to fit data from four Io flybys (I24 at 611 km, I25 at 300 km, I27 at 198 km, and I33 at 102 km). A satisfactory fit can be achieved with a second degree and order harmonic expansion for all the satellite flybys except G2, and for that one flyby even a third degree and order expansion leaves systematic Doppler residuals. The G2 flyby is unique.

The surface mass-point model provides a simple approach to fitting the data. Further analysis will be required to determine if other mass anomalies at different locations and depths below the surface might also yield acceptable fits to the Doppler residuals. Our fitting model of point masses does not allow specification of the horizontal dimensions over which the density heterogeneities extend, although these are likely to be hundreds of kilometers, comparable to the distances from the anomalies to the spacecraft. With additional study of the point-mass model and incorporation of more realistic anomaly shapes (disks, spheres) into the analysis, it may be possible to identify the physical sources of the anomalies. If the anomalies are at the surface, or near to it, then they could be supported for a lengthy period of geological time by the cold and stiff outer layers of Ganymede's ice shell.

References and Notes
1. A compilation of satellite data can be found in D. J. Tholen, V. G. Tejfel, A. N. Cox, *Allen's Astrophysical Quantities*, A. N. Cox, Ed. (Springer-Verlag, New York, ed. 4, 2000), pp. 302–310.
2. The interior composition, structure, and dynamics of the four Galilean satellites have been summarized, along with a bibliography, by G. Schubert, J. D. Anderson, T. Spohn, W. B. McKinnon, in *Jupiter*, F. Bagenal, T. E. Dowling, W. B. McKinnon, Eds. (Cambridge Univ. Press, New York, 2004), chap. 13.
3. W. M. Kaula, *Theory of Satellite Geodesy* (Blaisdell, Waltham, MA, 1966).
4. J. D. Anderson *et al.*, Galileo Gravity Science Team, *Bull. Am. Astron. Soc.* **33**, 1101 (2001). This reference includes the best determination of Ganymede's radius currently available.
5. P. J. Mohr, B. N. Taylor, *Phys. Today* **55**, BG6 (2002). Because of recent determinations, the adopted value of G has fluctuated over the past few years. We use the current (2002) value recommended by the Committee on Data for Science and Technology (CODATA), $G = 6.6742 \times 10^{-11}$ m^3 kg^{-1} s^{-2}, with a relative standard uncertainty of 1.5×10^{-4}.
6. P. M. Muller, W. L. Sjogren, *Science* **161**, 680 (1968).
7. We acknowledge the work of Ö. Olsen for finding fits to the fourth-degree gravitational field. We thank W. L. Sjogren, A. S. Konopliv, and D.-N. Yuan for their assistance, especially for providing us with a recompiled version of their gravity-anomaly software *Gravity Tools*. We also thank D. Sandwell for helpful discussions about the nature of Ganymede's gravity anomalies, and S. Asmar, G. Giampieri, and D. Johnston for helpful discussions. This work was performed at the Jet Propulsion Laboratory, California Institute of Technology, under contract with NASA. G.S., W.B.M., and J.L.P. acknowledge support by grants from NASA through the Planetary Geology and Geophysics program.

Probing the Accumulation History of the Voluminous Toba Magma

Jorge A. Vazquez[1]*† and Mary R. Reid[1,2]

The age and compositional zonation in crystals from the Youngest Toba Tuff record the prelude to Earth's largest Quaternary eruption. We used allanite crystals to date and decipher this zoning and found that the crystals retain a record of at least 150,000 years of magma storage and evolution. The dominant subvolcanic magma was relatively homogeneous and thermally stagnant for ~110,000 years. In the 35,000 years before eruption, the diversity of melts increased substantially as the system grew in size before erupting 75,000 years ago.

Toba caldera, a continental arc volcano in Sumatra, Indonesia, produced Earth's largest Quaternary eruption, ejecting >3000 km^3 of magma 73,000 ± 4000 years ago (*1*). Atmospheric loading by aerosols and ash from the Toba eruption may have accelerated cooling of Earth's climate (*2*) and resulted in near-extinction of humans (*3*). How quickly this and other huge volumes of magma can amass is unclear, especially because large volumes of eruptible magma have not been detected beneath areas of active and/or long-lived magmatism (*4*, *5*). The rate of magma accumulation can dictate whether reservoirs of magma simply cool and solidify or persist at magmatic conditions (*6*, *7*), and may influence the probability of volcanic eruption and the characteristics of associated plutonic intrusions (*8*, *9*). A detailed record of magmatic evolution is that retained by the compositional zoning of major minerals (*10*, *11*), and this might reveal how magma chambers accumulate and change (*12*, *13*). However, current analytical techniques are not sufficiently sensitive to put the chemical zoning in major minerals into an absolute time frame. Hence, it is impossible to relate the zoning stratigraphy of one crystal to another or evaluate the age of magma associated with crystallization. Here we use a combination of in situ compositional and isotopic analyses on single crystals of a less abundant mineral, the epidote-group mineral allanite, to date and quantify compositional zoning within and between crystals in the Youngest Toba Tuff (YTT) and to establish how this voluminous magma evolved before eruption.

Allanite is a common accessory mineral in rhyodacitic and rhyolitic magmas and may have considerable compositional zoning in major and

[1]Department of Earth and Space Sciences, University of California, Los Angeles, CA 90095–1567, USA. [2]Department of Geology, Northern Arizona University, Flagstaff, AZ 86011, USA.

*To whom correspondence should be addressed. E-mail: jvazquez@ess.ucla.edu
†Present address: Department of Geological Sciences, California State University, Northridge, CA 91330–8266, USA.

minor elements. High Th concentrations (1 to 2 weight %) and a large degree of U-Th fractionation between allanite and melt make it ideal for in situ dating by ^{238}U-^{230}Th disequilibrium methods, with an age resolution of tens of thousands of years. Whereas individual zircons are also amenable to in situ dating (14), the composition of allanite is particularly sensitive to the differentiation of magma. The YTT is compositionally zoned from 68 to 77 weight % SiO_2, with the majority (>70%) of erupted magma being >73 weight % SiO_2 (15). Chesner (15) concluded that this diversity of compositions was largely produced by crystal fractionation. We analyzed allanites from a representative 75 weight % SiO_2 rhyolite with the UCLA high-resolution ion microprobe and an electron microprobe (16).

When the ^{238}U-^{230}Th isotope characteristics of the host rhyolite are used to estimate initial ^{230}Th/^{232}Th activity ratios, the cores of the YTT allanites are found to have crystallization ages ranging from 100 to 225 thousand years ago (ka), and most rims have ages identical to or within analytical error of the ~75-ka eruption age (17). Allanite compositions oscillate on scales of 10 to 30 μm (Fig. 1). The greatest compositional variations (factor of 2 to 3) are in elements that can be divided into two groups that covary inversely: One group contains Mg, La, Ce, Ca, Ti, and Al, and the other Mn, Y, Sm, Nd, Th, Pr, and Fe (table S2). The zoning cannot reflect growth in a boundary layer that was depleted or enriched in allanite-compatible elements because melt trapped in the growing allanites lack such depletions or enrichments (18).

Ratios between the concentrations of chemically similar elements that substitute into the same crystallographic site in allanite, such as between the light and middle rare earth elements, can mirror compositional changes in melt from which the allanite grew in the same way as, for example, the Fe/Mg ratio in olivine mirrors that of the melt from which it grew (19). Two ratios that vary by a factor of ~2 in the allanites are MnO/MgO and La/Nd (Fig. 1). Each traces a distinct component of fractionation in rhyolitic magmas (20) and is essentially not fractionated by kinetic effects or coupled substitution in allanite because elements within each pair are similarly sized and charged and fit in the same crystallographic site. The effect of increasing fractionation on the composition of allanite is to progressively lower La/Nd and increase MnO/MgO in response to concomitant changes in the host melt (Fig. 2).

The variations in La/Nd and MnO/MgO in YTT allanites correlate smoothly (Fig. 2). In some crystals, zoning is normal (trending to lower La/Nd and higher MnO/MgO) or reverse, but in more than two-thirds of them, it is oscillatory, with a near-rim trend to a similar, more evolved composition (Fig. 1). Even though these allanites are present in one of the most evolved YTT pumices, some compositions match those for representative allanites from the least evolved YTT rhyolite (Fig. 2). Reversals to less evolved compositions (lower MnO/MgO and higher La/Nd) are typically abrupt and correspond to irregular boundaries marking zones with contrasting tone in backscattered electron (BSE) images.

La/Nd and MnO/MgO exchange coefficients enable us to predict how the YTT allanite compositions are related to fractionation of their parental melts (Fig. 2). Estimated La/Nd and MnO/MgO ratios for the rhyolitic melts overlap those for erupted glasses reported by Chesner (15), and the variation can be related by ~45% fractional crystallization (Fig. 2). This is com-

parable to an estimate of 40 to 50% fractionation based on the major element variability of YTT pumices (15). Affinity between allanite compositions and YTT melts is further suggested by the agreement between measured and predicted melt concentrations for elements such as Mn and Mg (fig. S1).

The young age of the allanites shows that the YTT eruption tapped a rhyolitic magma produced after the demise of the preceding (Middle Toba Tuff, 500 ka) caldera magma chamber. In addition, the continuity of the growth record shows that the antiquity of the allanites is not due solely to preferential preservation and/or recycling of crystals from older intrusions. The ~35,000 to 150,000 years of magmatic evolution recorded by individual allanites is comparable to crystallization intervals estimated largely by zircon dating (21) of the other voluminous (>1000 km³) silicic magmas. Within this time frame, voluminous crystal-rich magmas can undergo fractionation differentiation by compaction and/or hindered crystal settling or can be thermally rejuvenated by an influx of mafic magma into the base of the subvolcanic reservoir (22, 23).

The oscillatory zoning and disparate histories of the allanite (Fig. 1) require heterogeneous conditions of crystallization, whether in mush (>40% crystals) or liquid-rich domains. The irregular boundaries and compositional reversals in the allanites are suggestive of episodic dissolution due to mixing with hotter, less evolved magmas. Crystals may have been cycled between distinct batches of magma in Toba's reservoir by differential movement along boundaries between convectional zones (24, 25) or mingling between recharge and resident magmas and/or during intrareservoir self-mixing (26, 27). Although the range in melt variation required by the allanite zoning does not require some of the crystallization to have occurred in magma mush,
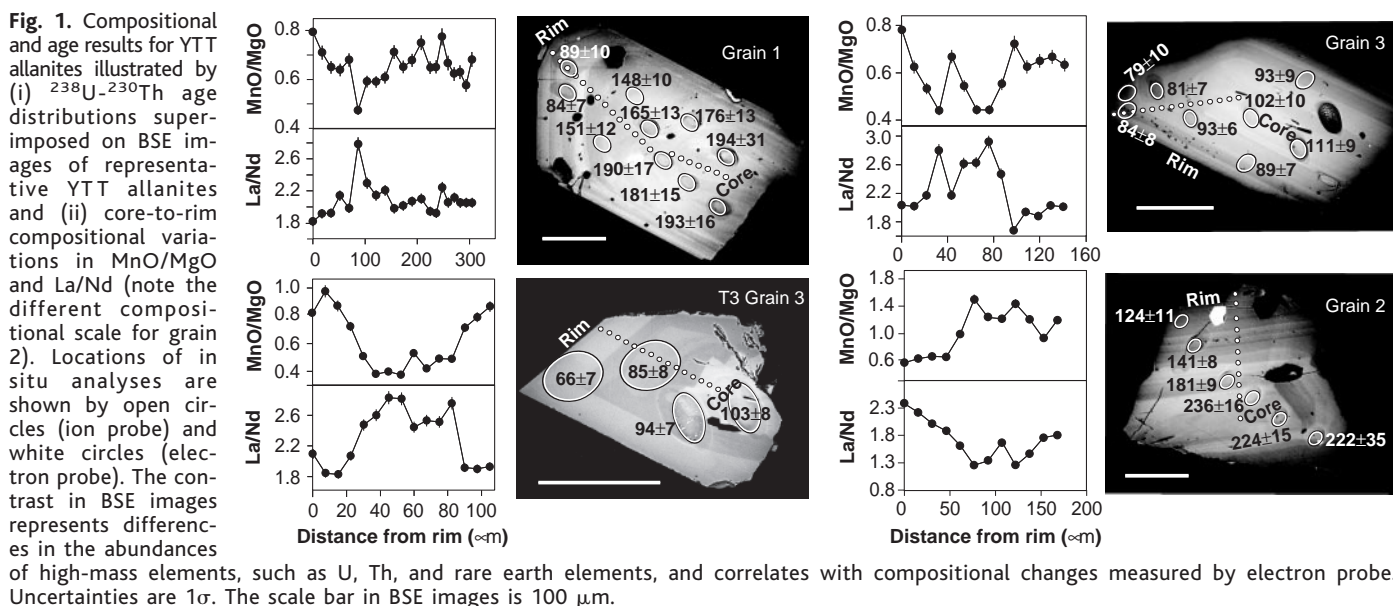

Fig. 1. Compositional and age results for YTT allanites illustrated by (i) ^{238}U-^{230}Th age distributions superimposed on BSE images of representative YTT allanites and (ii) core-to-rim compositional variations in MnO/MgO and La/Nd (note the different compositional scale for grain 2). Locations of in situ analyses are shown by open circles (ion probe) and white circles (electron probe). The contrast in BSE images represents differences in the abundances of high-mass elements, such as U, Th, and rare earth elements, and correlates with compositional changes measured by electron probe. Uncertainties are 1σ. The scale bar in BSE images is 100 μm.

it does not preclude it either, in which case the mush must have been periodically invaded by new silicic magma [compare (28)]. Evidently, magmatic conditions were frequently disrupted as the crystals grew, and the ages imply that greater disruption was closer to the time of eruption.

From ~225 to 110 ka, the allanite compositions are relatively restricted, excluding a single grain with evolved compositions (Fig. 3). Between ~110 and 75 ka, the compositional variability of the allanites is high. Only close to their rims do the allanite compositions converge (Figs. 1 and 3). On the basis of these patterns, we suggest that initially, and for a protracted interval of time, much of the Youngest Toba Tuff reservoir was relatively homogeneous, with melt compositions varying by <15% fractionation (or ~74 to 77 weight % SiO_2). The reservoir was nearly thermally stagnant, reflecting a heat balance perched between magmatic influxes and cooling of the system. Nearer to eruption, the diversity of melts sampled by the crystals increased substantially (melts related by up to 45% fractionation or ~70 to 77 weight %
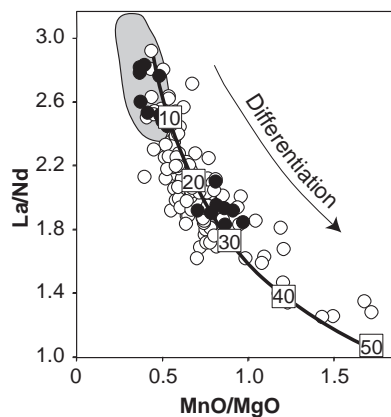
SiO_2). Mixing was probably less efficient as the system grew in size and diverse conditions of magma storage developed, resulting in domains of variably fractionated magmas and compositional zoning of the reservoir. Zoning of the magma that finally erupts (68 to 77 weight % SiO_2) could have developed even closer to eruption if the crystal-chemical variations arose in a mush rather than a liquid-dominated reservoir. Different magma batches may have intermittently coalesced in response to mass and heat input from the influx of new magma, as documented for the recent eruptions of Soufriere Hills and Rua-

pehu volcanoes (8, 29), or when melts were expelled by gravitational collapse of critically thickened batches of magma mush (22). The likely voluminous domains of not-yet rigid magma mush probably enhanced the likelihood of cumulate crystals being reentrained (12), but those rare crystals with distinct compositions were probably harvested from relatively isolated batches of magma that were even closer to solidification. Final merging of magma in the Toba reservoir, rather than the periodic recharge that sustained the magmatic system for >100,000 years, could have catalyzed the cataclysmic eruption.

Our results demonstrate that the components of a huge subvolcanic magma reservoir may unite crystals that probe magmatic evolution in space and time, and that intrusions of silicic magma may undergo a transition between homogeneous and heterogeneous states during their storage in Earth's crust. A corollary is that in chemically and/or isotopically zoned bodies of magma (10, 27), different crystal-zoning profiles may reflect spatial as well as temporal variations in the magma reservoir. Our results predict that the crystal-rich residue remaining after eruption of the YTT magma would form a compositionally zoned pluton that is locally monotonous but complexly zoned at a mineral scale, features that are increasingly observed in the plutonic record (12, 30). Because the YTT magma reservoir grew by piecemeal accumulation [compare (6, 7)] with mingling between successive additions of magma, crystals from domains of the reservoir that did not erupt, such as any cumulate pile underpinning the more liquid portions of the reservoir (31, 32), might record this evolution as well. Generation of the YTT magma by melting and remobilization of a young granitic pluton (33) is unlikely because the amount of crystallization recorded by the allanites is so much less than expected for solidification of an intrusion. Instead, the YTT magma accumulated and evolved over a period of >100,000 years.
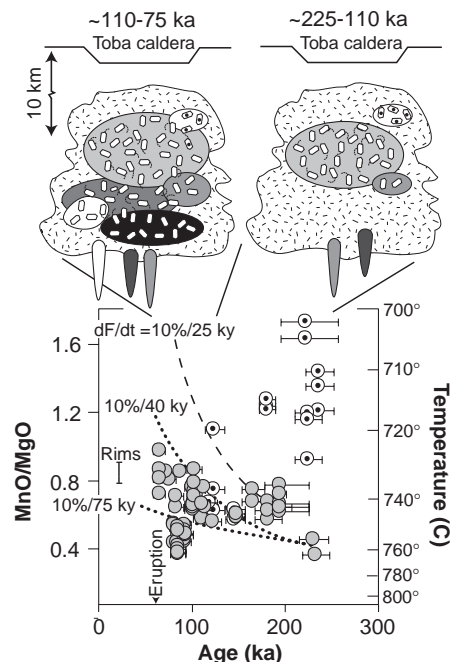

Fig. 3. Temporal variation in MnO/MgO for YTT allanites and cartoons depicting the magmachronology of rhyolite beneath Toba caldera. The depth of the system is from (15). Temperatures of magma during allanite growth are based on covariation of temperature and MnO/MgO reported by (44) for experimental crystallization of YTT magma compositions at 100 to 200 MPa. Reference to dashed curves for different rates of MnO/MgO fractionation (dF/dt = rate of crystal-liquid fractionation, starting at two different compositions recorded in the oldest allanite cores) based on the mineralogy the YTT emphasizes the divergence of the data from simple evolutionary trends. Most allanite compositions (gray circles) between ~225 and 110 ka are restricted and reflect a body of rhyolitic magma that is relatively invariant compositionally. Rare grains (e.g., grain 2) reflect isolated batches of highly evolved magmas (white circles with black dots). The increase in diversity of allanite composition between 110 and 75 ka is produced by the interaction and mingling of differentially fractionated batches of rhyolitic magma with temperatures between ~760° and 715°C. Final mixing (not shown) gathers crystals into the most evolved batch of rhyolite in the reservoir that then erupts at 75 ka.

Fig. 2. Plot of La/Nd versus MnO/MgO for allanites from evolved YTT rhyolite. Curve shows allanite compositions expected for crystallization from melts related by fractionating the quartz-plagioclase-sanidine-biotite phenocryst assemblage in modal proportions observed by (15), beginning from the least evolved melt composition. A La/Nd exchange coefficient, $D^{La/Nd}$, relating allanite composition to melt composition is 1.7 ± 0.1 [1 SD; computed from data of (38, 39)] and agrees well with values of 1.5 to 1.6 calculated by applying the model of Blundy and Wood (40) to the structural data of Dollase (41). $D^{La/Nd}$ is essentially constant over much of the range of low-to-high silica rhyolites, even though absolute partition coefficients increase. A $D^{MnO/MgO}$ value of 1.4 ± 0.3 (1 SD) based on data for high-silica rhyolites [data of (39, 42)] is less constrained because of a smaller number of partitioning data, but it agrees with the value of 1.4 based on the Blundy and Wood (40) model. Compositions in single grains (e.g., grain 3, black circles) may overlap nearly the entire range of observed allanite compositions, including allanites from the least evolved (68 weight % SiO_2) rhyolite (gray field) reported by (43).

References and Notes

1. C. A. Chesner, W. I. Rose, A. Deino, R. Drake, J. A. Westgate, *Geology* **19**, 200 (1991).
2. M. R. Rampino, S. Self, *Nature* **359**, 50 (1992).
3. M. R. Rampino, S. Self, *Science* **262**, 1955 (1993).
4. H. M. Iyer in, *Volcanic Seismology*, P. Gasparini, R. Scarpa, K. Aki, Eds. (Springer-Verlag, Berlin, 1992), pp. 299–338.
5. A. F. Glazner, J. M. Bartley, D. S. Coleman, W. Gray, R. Z. Taylor, *GSA Today* **14**, 4 (2004).
6. R. B. Hanson, A. F. Glazner, *Geology* **23**, 213 (1995).
7. A. S. Yoshinobu, D. A. Okaya, S. R. Paterson, *J. Struct. Geol.* **20**, 1205 (1998).
8. M. D. Murphy, R. S. J. Sparks, J. Barclay, M. R. Carroll, T. S. Brewer, *J. Petrol.* **41**, 21 (2000).
9. S. Blake, *Nature* **289**, 783 (1981).
10. J. P. Davidson, F. J. T. Tepley, *Science* **275**, 826 (1997).
11. G. S. Wallace, G. W. Bergantz, *Earth Planet. Sci. Lett.* **202**, 133 (2002).
12. J. Blundy, N. Shimizu, *Earth Planet. Sci. Lett.* **102**, 178 (1991).

13. A. T. Anderson, A. M. Davis, F. Lu, *J. Petrol.* **41**, 449 (2000).
14. M. R. Reid, C. D. Coath, T. M. Harrison, K. D. McKeegan, *Earth Planet. Sci. Lett.* **150**, 27 (1997).
15. C. A. Chesner, *J. Petrol.* **39**, 397 (1998).
16. Materials and analytical methods are available as supporting material on *Science* Online.
17. Model ^{238}U-^{230}Th ages are derived as described in (*14*). See (*34*) for a review of ^{230}Th dating in magmatic systems. The reported ages are taken to be those of crystallization because of the relatively tight packing of ions within allanite and the tetravalent charge of Th [compare (*35*)]. Reequilibration of Th during magmatic residence will be insignificant: Based on the predictive model of Fortier and Giletti (*36*), Th diffusion would only affect ~2 μm in allanite over a period of 100,000 years at the highest reported temperature of the YTT magma (~780°C). Uncertainty in the calculated ages due to possible variation of initial ^{230}Th/^{232}Th during magmatic evolution can be evaluated by assuming that observed eruption-age ^{230}Th/^{232}Th activity ratio variations of the YTT (0.358 to 0.433) are representative of the initial range of Th-isotope composition. For reported ages <120 ka, the uncertainty in age associated with the initial ratio is within the analytical uncertainty on the ages, except for the youngest allanite domains which could not have grown from melts that had Th isotope compositions significantly different from that of their host. Reported ages that are 120 to 200 ka could be at most a few percent to, for the older of these, as much as 27% older than allowed by the analytical uncertainty. Those few allanites with ages >200 ka could be substantially older. Thus, the age ranges reported here are conservative.
18. J. B. Thomas, R. J. Bodnar, N. Shimizu, C. Chesner, in *Zircon*, J. M. Hanchar, P. W. O. Hoskin, Eds. (Mineralogical Society of America, Washington, DC, 2004), vol. 53, chap. 3.
19. P. L. Roeder, R. F. Emslie, *Contrib. Mineral. Petrol.* **29**, 275 (1970).
20. MnO/MgO in residual melts of silicic magmas typically increases with fractionation of major mafic silicates. La/Nd also increases except when the fractionating assemblage includes sufficient quantities of allanite, chevkinite, and/or monazite that are rich in light rare earth elements (*37*).
21. M. R Reid, in *Treatise on Geochemistry*, H. D. Holland, K. K Turekian, Eds. (Elsevier, Amsterdam, 2003), vol. 3, chap. 3.05.
22. O. Bachmann, G. W. Bergantz, *J. Petrol.*, **45**, 1565 (2004).
23. O. Bachmann, G. W. Bergantz, *Geology* **27**, 447 (2003).
24. B. D. Marsh, M. R. Maxey, *J. Volcanol. Geotherm. Res.* **24**, 95 (1985).
25. V. R. Troll, H. U. Schmincke, *J. Petrol.* **43**, 243 (2002).
26. G. W. Bergantz, *J. Struct. Geol.* **22**, 1297 (2000).
27. S. Couch, R. S. J. Sparks, M. R. Carroll, *Nature* **411**, 1037 (2001).
28. S. Turner, R. George, D. A. Jerram, N. Carpenter, C. Hawkesworth, *Earth Planet. Sci. Lett.* **214**, 279 (2003).
29. M. Nakagawa, K. Wada, T. Thordarson, C. P. Wood, J. A. Gamble, *Bull. Volcanol.* **61**, 15 (1999).
30. D. M. Robinson, C. F. Miller, *Am. Mineral.* **84**, 1346 (1999).
31. C. A. Bachl, C. F. Miller, J. S. Miller, J. E. Faulds, *GSA Bull.* **113**, 1213 (2001).
32. T. H. Druitt, C. R. Bacon, *Trans. R. Soc. Edinburgh Earth Sci.* **79**, 289 (1988).
33. I. N. Bindeman, J. W. Valley, *Geology* **28**, 719 (2000).
34. M. Condomines, P.-J. Gauthier, O. Sigmarsson, in *Uranium-Series Geochemistry*, B. Bourdon, G. M. Henderson, C. C. Lundstrom, S. P. Turner, Eds. (Mineralogical Society of America, Washington, DC, 2003), vol. 52, chap. 4.
35. E. Dowty, *Am. Mineral.* **65**, 174 (1980).
36. S. M. Fortier, B. J. Giletti, *Science* **245**, 1481 (1989).
37. C. F. Miller, D. W. Mittlefehldt, *Geology* **10**, (1982).
38. C. K. Brooks, P. Henderson, J. G. Ronsbo, *Mineral. Mag.* **44**, 157 (1981).
39. G. A. Mahood, W. Hildreth, *Geochim. Cosmochim. Acta* **47**, 11 (1983).
40. J. Blundy, B. Wood, *Nature* **372**, 452 (1994).
41. W. A. Dollase, *Am. Mineral.* **56**, 447 (1971).
42. A. Ewart, W. L. Griffin, *Chem. Geol.* **117**, 251 (1994).
43. C. A. Chesner, A. D. Ettlinger, *Am. Mineral.* **74**, 750 (1989).
44. J. E. Gardner, P. W. Layer, M. J. Rutherford, *Geology* **30**, 347 (2002).

More Intense, More Frequent, and Longer Lasting Heat Waves in the 21st Century

Gerald A. Meehl* and Claudia Tebaldi

A global coupled climate model shows that there is a distinct geographic pattern to future changes in heat waves. Model results for areas of Europe and North America, associated with the severe heat waves in Chicago in 1995 and Paris in 2003, show that future heat waves in these areas will become more intense, more frequent, and longer lasting in the second half of the 21st century. Observations and the model show that present-day heat waves over Europe and North America coincide with a specific atmospheric circulation pattern that is intensified by ongoing increases in greenhouse gases, indicating that it will produce more severe heat waves in those regions in the future.

There is no universal definition of a heat wave, but such extreme events associated with particularly hot sustained temperatures have been known to produce notable impacts on human mortality, regional economies, and ecosystems (*1–3*). Two well-documented examples are the 1995 Chicago heat wave (*4*) and the Paris heat wave of 2003 (*5*). In each case, severe hot temperatures contributed to human mortality and caused widespread economic impacts, inconvenience, and discomfort.

In a future warmer climate with increased mean temperatures, it seems that heat waves would become more intense, longer lasting, and/or more frequent (*6, 7*). However, analyses of future changes in other types of extreme events, such as frost days, show that changes are not evenly distributed in space but are characterized instead by particular patterns related to larger scale climate changes (*8*). Here, we examine future behavior of heat waves in a global coupled climate model, the Parallel Climate Model (PCM). This model has a latitude-longitude resolution of about 2.8° in the atmosphere and a latitude-longitude resolution of less than 1° in the ocean, and it contains interacting components of atmosphere, ocean, land surface, and sea ice. The PCM has been used extensively to simulate climate variability and climate change in a variety of applications for 20th- and 21st-century climate (*6, 8–13*). We analyzed a four-member ensemble (i.e., the model was run four

times from different initial states and the four members were averaged together to reduce noise) for 20th-century climate and a five-member ensemble for 21st-century climate. The former includes the major observed forcings for the 20th century encompassing greenhouse gases, sulfate aerosols, ozone, volcanic aerosols, and solar variability (*13*). The latter uses a "business-as-usual" scenario, which assumes little in the way of policy intervention to mitigate greenhouse gas emissions in the 21st century (*14*). We define the present-day reference period as 1961 to 1990 for model and observations and the future as the time period from 2080 to 2099.

First, we sought to define a heat wave. Many definitions could apply to heat waves that quantify the duration and/or intensity of either nighttime minima or daytime maxima (*4, 5, 15, 16*). Here, we used two definitions of heat waves; each has been shown to be associated with substantial societal impacts on human health and economies. The first (*4*) evolved from a study of the 1995 Chicago heat wave; it concentrates on the severity of an annual "worst heat event" and suggests that several consecutive nights with no relief from very warm nighttime minimum temperatures may be most important for health impacts. For present-day climate for North America and Europe (Fig. 1), the means of three consecutive warmest nights for observations and the model show good agreement. Heat waves presently are more severe in the southeast United States (large areas greater than 24°C) and less severe in the northwest United States (equally large areas less than 16°C; Fig. 1, A and C). For Europe, there is more of a north-south gradient in both obser-

National Center for Atmospheric Research (NCAR), Post Office Box 3000, Boulder, CO 80307, USA.

*To whom correspondence should be addressed. E-mail: meehl@ncar.ucar.edu